

From Micro- to Macro-scales in the Heliosphere and Magnetospheres

Dastgeer Shaikh¹, I. S. Veselovsky^{2,3}, Q. M. Lu⁴, G.P. Zank¹

Abstract From a broader perspective, the heliosphere and planetary magnetospheres provide a test bed to explore the plasma physics of the Universe. In particular, the underlying nonlinear coupling of different spatial and temporal scales plays a key role in determining the structure and dynamics of space plasmas and electromagnetic fields. Plasmas and fields exhibit both laminar and turbulent properties, corresponding to either well organized or disordered states, and the development of quantitative theoretical and analytical descriptions from physics based first principles is a profound challenge. Limited observations and complications introduced by geometry and physical parameters conspire to complicate the problem. Dimensionless scaling analysis and statistical methods are universally applied common approaches that allow for the application of related ideas to multiple physical problems. We discuss several examples of the interplay between the scales in a variety of space plasma environments, as exemplified in the presentations of the session *From Micro- to Macro-scales in the Heliosphere and Magnetospheres*.

1 Turbulent spectra in the solar wind and interstellar medium

The solar wind and interstellar medium is predominantly in a turbulent state (Marsch E. & C.-Y. Tu 1995; Goldstein et al 1995; Bruno & Carbone 2005) in which low frequency fluctuations are described typically by a magnetohydrodynamics (MHD) description of plasma. Nonlinear interactions amongst these fluctuations lead to a migration of energy in the inertial range that is characterized typically by a

¹Center for Space Plasma and Aeronomic Research and Physics Department, University of Alabama, Huntsville, AL 35899, USA e-mail: \protect\protect\protect\edefOT1{OT1}\let\enc@update\relax\protect\edefptm{ptm}\protect\edefm{

²Skobel'syn Institute of Nuclear Physics, Moscow State University, Moscow, 119992, Russia ·

³Space Research Institute (IKI), Russian Academy of Sciences, Moscow, 117997, Russia · ⁴CAS Key Laboratory of Basic Plasma Physics, School of Earth and Space Sciences, University of Science and Technology of China, Hefei, Anhui, 230026, China

Kolmogorov-like 5/3 spectrum (Frisch 1995). The 5/3 power spectrum is observed frequently, both in the interstellar medium (ISM) and solar wind (SW). The ubiquity of the turbulence spectrum on a variety of length scales, leading to a Kolmogorov-like 5/3 law, is one of the long standing puzzles of classical statistical theories of turbulence, the origin and nature of which remains a topic of considerable debate. Owing to its complexity, magnetized plasma turbulence in general is not only lacking substantially in theoretical developments because of its analytically intractable nature, but it also poses computationally a challenging task of resolving multiple scale flows and fluctuations that are best described statistically. The fields of plasma and hydrodynamic turbulence have grown tremendously with the advent of high speed supercomputing and efficient numerical algorithms. It is not possible to cover all aspects of the field in this article, and so we concentrate mainly on the physical processes that lead to the 5/3 spectra in both ISM and SW plasmas. Understanding energy cascade processes is important particularly from the point of view of non-linear interactions across disparate scales, turbulence transport, wave propagation, heating processes in the solar wind, structure formation, cosmic ray scattering, and particle acceleration throughout the heliosphere.

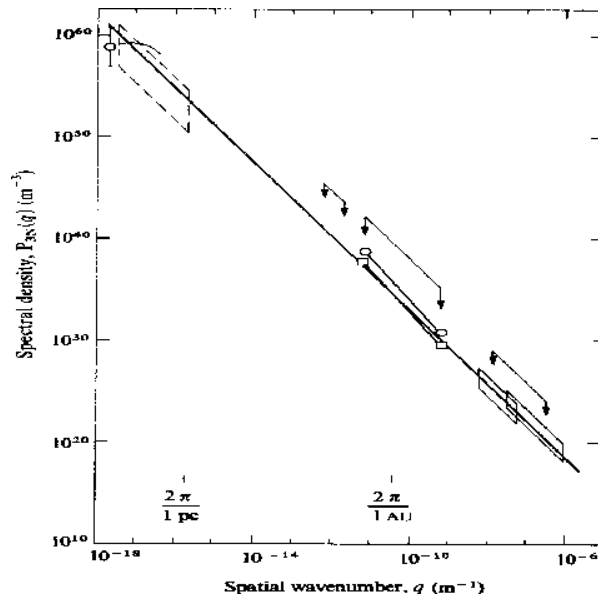


Fig. 1 ISM turbulence spectrum exhibiting a 5/3 power law (Armstrong et al 1981).

1.1 Turbulence spectra in the interstellar medium

It is a curious observation (Fig 1) that electron density fluctuations in the interstellar medium (ISM) exhibit an omnidirectional Kolmogorov-like (Kolmogorov 1941) power spectrum $k^{5/3}$ (or $11/3$ spectra index in three dimensions) over a 4 to 6 decade range (Armstrong, Cordes & Rickett 1981; Higdon 1984, 1986; Armstrong et al. 1990). The observed turbulence spectrum extends over an extraordinary range of scales i.e. from an outer scale of a few parsecs to scales of few AUs or less. Interstellar scintillation, describing fluctuations in the amplitude and phase of radio waves caused by scattering in the interstellar medium, exhibit the power spectrum of the interstellar electron density that follows a $5/3$ index (Armstrong, Rickett & Spangler 1995). The origin and nature of this big power law is described in an extensive review by Elmegreen & Scalo (2004). Chepurnov & Lazarian (2010) used the data of the Wisconsin H α Mapper (WHAM) and determined that the amplitudes and spectra of density fluctuations can be matched to the data obtained for interstellar scintillations and scattering that follow a Kolmogorov-like spectrum spanning from 106 to 1017 m scales. Angular broadening measurements also reveal, more precisely, a Kolmogorov-like power spectrum for the density fluctuations in the interstellar medium with a spectral exponent slightly steeper than $-5/3$ (Mutel et al, 1998; Spangler, 1999). Regardless of the exact spectral index, the density irregularities exhibit a power-law spectrum that is essentially characteristic of a fully developed isotropic and statistically homogeneous incompressible fluid turbulence, described by Kolmogorov (1941) for hydrodynamic and Kraichnan (1965) for magnetohydrodynamic fluids. Turbulence, manifested by interstellar plasma fluid motions, therefore plays a major role in the evolution of the ISM plasma density, velocity, magnetic fields, and the pressure. Radio wave scintillation data indicates that the rms fluctuations in the ISM and interplanetary medium density, of possibly turbulent origin and exhibiting Kolmogorov-like behavior, are only about 102001). This suggests that ISP density fluctuations are only weakly compressible. Despite the weak compression in the ISP density fluctuations, they nevertheless admit a Kolmogorov-like power law, an ambiguity that is not yet completely resolved by any fluid/kinetic theory or computer simulations. That the Kolmogorov-like turbulent spectrum stems from purely incompressible fluid theories (Kolmogorov, 1941; Kraichnan, 1965) of hydrodynamics and magnetohydrodynamics offers the simplest possible turbulence description in an isotropic and statistically homogeneous fluid. However, since the observed electron density fluctuations in the ISM possess a weak degree of compression, the direct application of such simplistic turbulence models to understanding the ISM density spectrum is not entirely obvious. Moreover, the ISM is not a purely incompressible medium and can possess many instabilities because of gradients in the fluid velocity, density, magnetic field etc. where incompressibility, inhomogeneity and even isotropy are certainly not good assumptions. This calls for a fully self-consistent description of ISM fluid, one that couples incompressible modes with weakly compressible modes and deals with the strong nonlinear interactions amongst the ISM density, temperature, velocity and the magnetic field. Note

that the coupling of different modes is an intrinsic property of MHD perturbations of finite amplitude.

1.2 Solar wind turbulence spectra

Solar wind plasma, on the other hand, occurs on much smaller scales, i.e. few thousands of kilometers, compared to the ISM scales. A wealth of data from in-situ observations is available from numerous spacecraft and reveals the nonlinear turbulent character of the magnetized solar wind plasma fluid. It is evident from these observations that the solar wind plasma yields a multitude of spatial and temporal length-scales associated with an admixture of waves, fluctuations, structures and nonlinear turbulent interactions. In-situ measurements (Matthaeus & Brown 1988, Goldstein et al 1994, 1995, Ghosh et al 1996) indicate that solar wind fluctuations, extend over several orders of magnitude in frequency and wavenumber. The fluctuations can be described by a power spectral density (PSD) spectrum that can be divided into three distinct regions (Goldstein et al 1995, Leamon et al 1999) depending on the frequency and wavenumber. This is shown in the schematic of Fig 2. The first region corresponds to a flatter spectrum, associated with lower frequencies consistent with a k^{-1} (where k is wavenumber) power law. A second identifiable region follows and extends to the ion/proton gyrofrequency, with a spectral slope that has an index ranging from $-3/2$ to $-5/3$. This region is identified with fully developed turbulence, and is generally described on the basis of the incompressible magnetohydrodynamic (MHD) equations. The turbulent interactions in this regime are thought to be governed entirely by Alfvénic cascades. Spacecraft observations (Leamon et al 1999, Bale et al. 2005, Alexandrova et al 2007, 2008, Sahraoui et al 2007, 2009) further reveal that at length scales beyond the MHD regime, i.e. length scales less than ion gyro radius $k\rho_i < 1$ and temporal scales greater than the ion cyclotron frequency $\omega > \omega_{ci} = eB_0/m_e c$ (where $k, \rho_{ci}, e, B_0, m_e, c$ are respectively characteristic mode, ion gyroradius, ion cyclotron frequency, electronic charge, mean magnetic field, mass of electron, and speed of light), the spectrum exhibits a spectral break, and the spectral index of the solar wind turbulent fluctuations varies between -2 and -5 (Smith et al 2006, Goldstein et al 1994, Leamon et al 1999, Bale et al. 2005, Shaikh & Shukla 2008, 2009, Sahraoui et al 2009). Higher time resolution observations find that at the spectral break, Alfvénic MHD cascades (Smith et al 2006, Goldstein et al 1994, Leamon et al 1999) close. The characteristic modes in this region appear to evolve typically on timescales associated with dispersive kinetic Alfvénic fluctuations.

The onset of the second or the kinetic Alfvén inertial range is not understood. Some suggestions have however been made. The spectral break may result from energy transfer processes associated with possibly kinetic Alfvén waves (KAWs) (Hasegawa 1976), electromagnetic ion- cyclotron-Alfvén (EMICA) waves (e.g., Gary, 2008) or by fluctuations described by a Hall MHD (HMHD) plasma model (Alexandrova et al 2007, 2008; Shaikh & Shukla 2008, 2008a). Stawicki et al

(2001) argue that Alfvén fluctuations are suppressed by proton cyclotron damping at intermediate wavenumbers so the observed power spectra are likely to comprise weakly damped dispersive magnetosonic and/or whistler waves. Beinroth & Neubauer (1981) and Denskat & Neubauer (1982) have reported the presence of whistler waves based on Helios 1 and 2 observations in this high frequency regime. A comprehensive data analysis by Goldstein et al. (1994), based on correlations of sign of magnetic helicity with direction of magnetic field, indicates the possible existence of multiscale waves (Alfvénic, whistlers and cyclotron waves) with a single polarization in the dissipation regime. Counter-intuitively, in the $\omega < \omega_{ci}$ regime, or Alfvénic regime, Howes et al. (2008) noted the possibility that highly obliquely propagating KAWs are present (with $\omega > \omega_{ci}$) making it questionable that damping of ion cyclotron waves is responsible for the spectral breakpoint.

Fluid (Shaikh & Zank 2010) and kinetic (Howes et al. 2008) simulations, in qualitative agreement with spacecraft data described as above, have been able to obtain the spectral break point near the characteristic turbulent length scales that are comparable with the ion inertial length scale (d_i). These simulations find Kolmogorov-like $k^{-5/3}$ spectra for length scales larger than ion inertial length scales, where MHD is typically a valid description. By contrast, smaller (than d_i) scales were shown to follow a steeper spectrum that is close to $k^{-7/3}$ (Howes et al. 2008, Shaikh & Shukla 2009). Spacecraft data and simulations thus reveal that migration of turbulent energy proceeds essentially through different regions in k-space, i.e. k^{-1} , $k^{-5/3}$ and $k^{-7/3}$. Of course, the turbulent cascade does not entirely terminate immediately beyond the $k^{-7/3}$ regime. Fluid and kinetic simulations (Biskamp 1996, Galtier 2006, Galtier & Buchlin 2007, Cho & Lazarian 2003, Shaikh & Zank 2005, Shaikh 2009, Gary et al. 2008, Saito et al. 2008, Howes et al. 2008) show that spectral transfer of energy extends even beyond the $k^{-7/3}$ regime and is governed predominantly by small scale, high frequency, whistler turbulence. The latter also exhibits a power law.

1.3 Extended composite spectra of the solar wind plasma

Theory and simulations indicate that turbulent fluctuations in the high frequency and $k\rho_i > 1$ regime correspond to electron motions that are decoupled from the ion motions (Kingsep et al 1990, Biskamp et al 1996, Shaikh et al 2000a, Shaikh et al 2000b, Shaikh & Zank 2003, Cho & Lazarian 2004, Saito et al 2008, Gary et al 2008). Correspondingly, ions are essentially unmagnetized and can be treated as an immobile neutralizing background fluid. This regime corresponds to the whistler wave band of the spectrum and comprises characteristic scales that are smaller than those that describe MHD, KAW or Hall MHD processes. An extended composite schematic describing the whistler mode spectra is also shown in Fig 2. Specifically, regions IV and V in Fig. 2 identify characteristic modes that are relevant for the description of whistler wave turbulence (Biskamp et al 1996, Shaikh & Zank 2005, Shaikh 2009). The boundary of regions III and IV represents a wavenumber band in spectral space that corresponds to the decoupling of electron and ion motions.

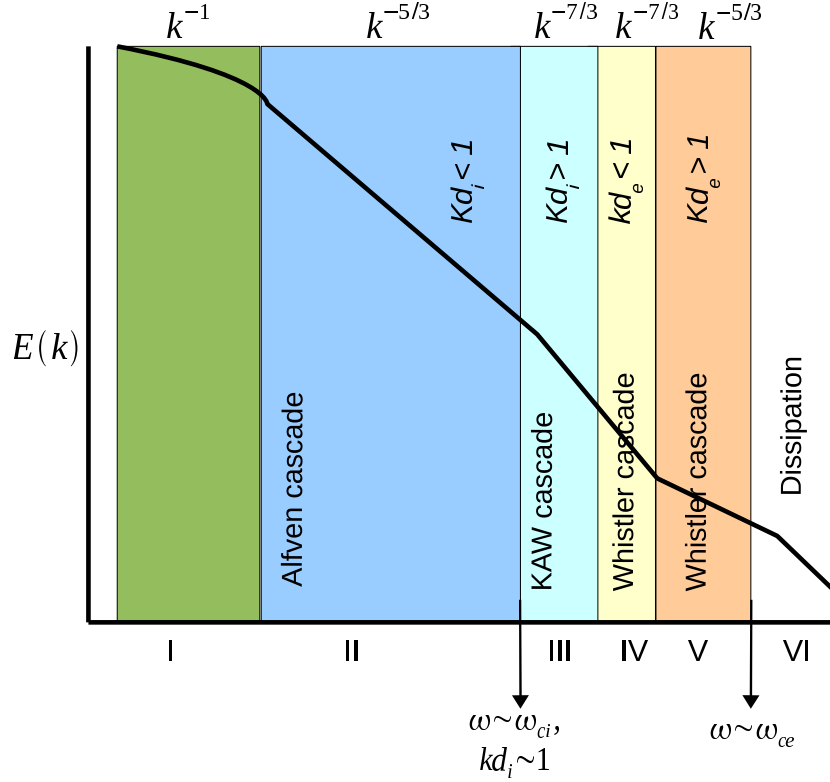


Fig. 2 Schematic of the power spectral density (PSD) composite spectrum in the solar wind turbulent plasma as a function of frequency (wavenumber). Several distinct regions are identified with what is thought to be the dominant energy transfer mechanism for that particular region. The non-linear processes associated with the transition from region II (MHD regime) to region III (kinetic or Hall MHD regime) are not yet fully understood. The power spectra in region III vary from k^{-2} to k^{-4} . The boundary of region III and IV identifies where electron and ion motions are decoupled. Regions IV and V are identified as whistler cascade regimes. The outerscale of MHD turbulence corresponds to the smaller k mode in region II which can possibly extend over a few parsecs in the context of ISM (Armstrong et al 1981).

Wavenumbers above this boundary characterize the onset of whistler turbulence. The spectral cascades associated with whistler turbulence are described extensively by Biskamp et al (1996), Shaikh et al (2000a), Shaikh et al (2000b), Shaikh & Zank (2003, 2005), Shaikh (2009a,b). Cho & Lazarian 2004 describe scale dependent anisotropy that is mediated by whistler waves in the context of electron MHD plasma. Gary et al. (2008) and Saito et al. (2008) have reported two-dimensional electromagnetic particle-in-cell simulations of an electron MHD model to demonstrate the forward cascade of whistler turbulence. Their work shows that the magnetic spectra of the cascading fluctuations become more anisotropic with increasing fluctuation energy. Interestingly, whistler turbulence associated with longer wavelengths in region IV exhibits a power spectrum $k^{-7/3}$ that is similar to the short

wavelength spectrum of kinetic Alfvén waves (KAW), as shown in region III of Fig 2. The underlying physical processes responsible for the spectrum differ significantly for KAW and whistler waves.

The Hall MHD description of magnetized plasma is valid up to region III where characteristic turbulent scales are smaller than ion inertial length scales ($kd_i > 1$). Beyond this location, high frequency motion of plasma is governed predominantly by electron motions, and ions form a stationary neutralizing background. Consequently, the ion motions decouple significantly from electron motion. These aspects of the spectra, depicted by regions IV & V in Fig 2, can be described adequately by whistler wave model. The Hall MHD models are therefore not applicable in regions IV, V and beyond. Neither can they describe kinetic physics associated with the dissipative regime. Since the high frequency regime (i.e. regions IV & V) is dominated by electron motions, there exists an intrinsic length scale corresponding to the electron inertial length scale $d_e = c/\omega_{pe}$ (where ω_{pe} is the electron plasma frequency). The characteristic turbulent length scales in regions IV & V are comparable with d_e and therefore describe scales larger (i.e. $kd_e < 1$ in region IV) and smaller (i.e. $kd_e > 1$ in region V) than the electron inertial scale. While whistler wave models can describe nonlinear processes associated with length scales as small as the electron inertial length scale, they fail to describe finite electron Larmor radius effects for which a fully kinetic description of plasma must be used.

Beside those issues described above, we do not understand what leads to the decoupling of ion and electron motions near the boundary of region III and IV for example. Although the turbulent spectra are described by similar spectral indices, the nonlinear processes are fundamentally different in region III and IV.

1.4 A nearly incompressible description of the SW and ISM spectra- the 5/3 MHD regime

Earlier fluid models, describing the turbulent motion of a compressible ISM fluid, have been based mostly on isothermal and adiabatic assumptions, due largely to their tractability in terms of mathematical and numerical analysis. Unfortunately, such models cannot describe the complex nonlinear dynamical interactions amongst ISM fluctuations self-consistently. For instance, density fluctuations, in the context of related solar wind work, were thought to have originated from nonlinear Alfvén modes (Spangler, 1987). A simple direct relationship of density variations with Alfvénic fluctuations is not entirely obvious as the latter are not fully self-consistent and are incompressible by nature thereby ignoring effects due to magnetoacoustic perturbations for example. On the other hand, fully compressible nonlinear MHD solutions, for both high- and low-cases, show that Alfvén and slow modes exhibit a $k^{-5/3}$ spectrum, while fast modes follow a $k^{-3/2}$ spectrum (Cho & Lazarian 2002, 2003). The formation of density power spectrum in the simulations of isothermal MHD turbulence was studied in Cho & Lazarian (2003), Beresnyak, Lazarian & Cho (2005), Kowal, Lazarian & Beresnyak (2008). In particular, in Beresnyak et al.

(2005), the logarithm of density was shown to follow the Goldreich-Sridhar scaling in terms of both density and anisotropy. This is an important finding that sheds the light onto the nature of the density fluctuations.

One of the most debated issues in the context of solar wind turbulence is the non-equipartition between the kinetic and magnetic part of the energies that leads to a discrepancy between the two spectra. The kinetic as well as magnetic energy spectra for fast or slow modes nevertheless do not relate to a Kolmogorov-like density spectrum. The latter modes have been suggested as candidates for generating density fluctuations (Lithwick & Goldreich, 2001) in the interstellar medium. Alternate explanations are that density structures (anisotropic) in the ISM emerge from pressure-balance stationary modes of MHD (also called Pressure Balance Structures, PBS) (Higdon, 1986), or from inhomogeneities in the large-scale magnetic field via the four-field model of Bhattacharjee et al. (1998). These descriptions are inadequate for a general class of ISM problems. The PBSs form a special class of MHD solutions and are valid only under certain situations when the magnetic and the pressure fluctuations exert equal forces in the stationary state. These structures, limited in their scope to the general ISM conditions, nevertheless do not offer an entirely self-consistent explanation to the observed density spectrum. Similarly, an inertial range turbulent cascade associated with the low turbulent Mach number four field MHD model is not yet known. Moreover this isothermal inhomogeneous fluid model is valid only for a class of MHD solutions and yields a linear Mach number (M) scaling, $O(M)$, amongst the various fluctuations (Bhattacharjee et al., 1998).

One of the earlier attempts to understand the ISM density fluctuations, and relate it to an incompressible fluid turbulence model dates back Montgomery et al. (1987) who used an assumed equation of state to relate ISM density fluctuations to incompressible MHD. This approach, called a pseudosound approximation, assumes that density fluctuations are proportional to the pressure fluctuations through the square of sound speed. The density perturbations in their model are therefore “slaved” to the incompressible magnetic field and the velocity fluctuations. This hypothesis was further contrasted by Bayly et al. (1992) on the basis of their 2D compressible hydrodynamic simulations by demonstrating that a spectrum for density fluctuations can arise purely as a result of abandoning a barotropic equation of state, even in the absence of a magnetic field. The pseudosound fluid description of compressibility, justifying the Montgomery et al. approach to the density-pressure relationship, was further extended by Matthaeus and Brown (1988) in the context of a compressible magnetofluid (MHD) plasma with a polytropic equation of state in the limit of a low plasma acoustic Mach number (Matthaeus and Brown, 1988). The theory, originally describing the generation of acoustic density fluctuations by incompressible hydrodynamics (Lighthill, 1952), is based on a generalization of Klainerman and Majda’s work (Klainerman and Majda, 1981, 1982; Majda, 1984) and accounts for fluctuations associated with a low turbulent Mach number fluid, unlike purely incompressible MHD. Such a nontrivial departure from the incompressible state is termed “nearly incompressible.” The primary motivation behind NI fluid theory was to develop an understanding and explanation of the interstellar scintillation observations of weakly compressible ISM density fluctuations that exhibit a Kolmogorov-

like power law. The NI theory is, essentially, an expansion of the compressible fluid or MHD equations in terms of weak fluctuations about a background of strong incompressible fluctuations. The expansion parameter is the turbulent Mach number. The leading order expansion satisfies the background incompressible hydrodynamic or magnetohydrodynamic equations (and therefore fully nonlinear) derived on the basis of Kreiss principle (Kreiss, 1982), while the higher order yields a high frequency weakly compressible set of nonlinear fluid equations that describe low turbulent Mach number compressive HD as well as MHD effects. Zank and Matthaeus derived the unified self-consistent theory of nearly incompressible fluid dynamics for non-magnetized hydrodynamics as well as magnetofluids, with the inclusion of the thermal conduction and energy effects, thereby identifying different and distinct routes to incompressibility (Zank & Matthaeus, 1991, 1993). In the NI theory, the weakly perturbed compressive fluctuations (denoted by subscript 1) are expanded about the incompressible modes (denoted by superscript 1) for velocity and pressure variables as $U = U^\infty + \varepsilon U_1$, $p = p_0 + \varepsilon^2(p^\infty + p_1)$ respectively. Here ε is a small parameter associated with the turbulent fluid Mach number M_s through the relation $C_s^2 = \gamma p / \rho$, $M_s = U_0 / C_s$ and γ is the ratio of the specific heats, U_0 is the characteristic speed of the turbulent fluid, and C_s is the acoustic speed associated with sound waves. Due to a lack of uniqueness in the representation of the fluid density and temperature fields, either of the choices $T = T_0 + \varepsilon T_1$ or $T = T_0 + \varepsilon^2 T_1$ is consistent. The first choice corresponds to a state where temperature fluctuations dominate both the incompressible and compressible pressure and is referred to as the heat fluctuation dominated (HFD) regime. On the other hand the second choice in which all the variables are of similar order is described as the heat fluctuation modified (HFM) regime. Since the thermal fluctuations in HFD regime appear at an order $O(\varepsilon)$ as compared with the pressure $O(\varepsilon^2)$, they dominate the NI ordering. By contrast, the thermal fluctuations have the same ordering with respect to the other fluctuations (density, pressure etc) in a HFM regime. The NI theory introduces a further fundamentally different explanation for the observed Kolmogorov-type density spectrum in that the ISM density fluctuations can be a consequence of passive scalar convection due to background incompressible fluctuations as well as a generalized pseudo-sound theory. The theory further predicts various correlations between the density, temperature and the acoustic as well as convective pressure fluctuations (Zank & Matthaeus, 1991, 1993, Shaikh & Zank 2005, 2006, 2007).

The validity and nonlinear aspects of the NI model, within the context of the interstellar medium, has recently been explored by Shaikh & Zank (2003, 2005, 2006, 2007, 2010). The theory of nearly incompressible (NI) fluids, developed by Matthaeus, Zank and Brown, based on a perturbative expansion technique is a rigorous theoretical attempt to understand the origin of weakly compressible density fluctuations in the interstellar medium, and one that provides formally a complete fluid description of ISM turbulence with the inclusion of thermal fluctuations and the full energy equation self-consistently, unlike the previous models described above (Zank & Matthaeus, 1990, 1991, 1993; Matthaeus and Brown, 1988). Owing to its broad perspective and wide range of applicability for interstellar medium problems, we use here a nearly incompressible description of fluids to investigate interstellar

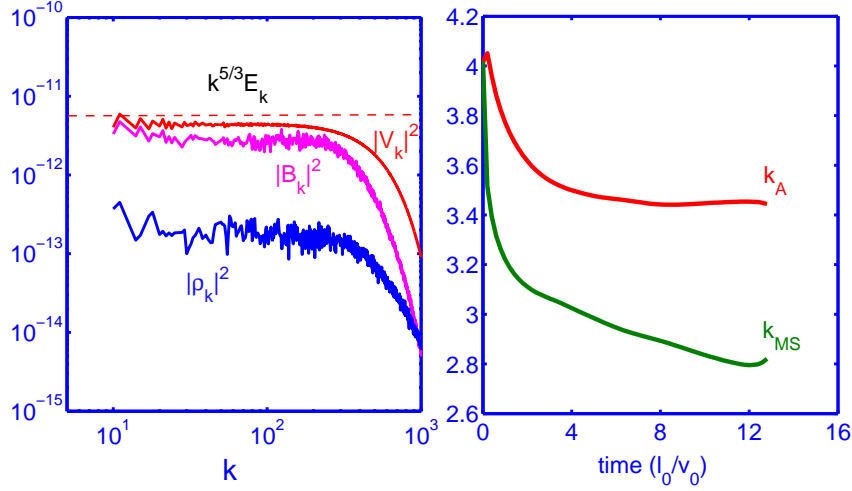


Fig. 3 (Left) Velocity fluctuations are dominated by shear Alfvenic motion and thus exhibit a Kolmogorov-like $k^{-5/3}$ spectrum. The middle curve shows the magnetic field spectrum. Density fluctuations are passively convected by the nearly incompressible shear Alfvenic motion and follow a similar spectrum in the inertial range. The numerical resolution in 3D is 512^3 . (Right) The evolution of Alfvenic (k_A) and fast/slow magnetosonic (k_{MS}) modes demonstrates that the spectral cascades are dominated by Alfvenic modes.

turbulence with a view to explaining the observed Kolmogorov-like ISM density spectrum. A central tenant of the homogeneous NI theory is that the density fluctuations are of higher order, of higher frequency and possess smaller length-scales than their incompressible counterparts to which they are coupled through passive convection and the low frequency generation of sound. Most recently, Hunana & Zank 2006, 2010 have extended the NI hydrodynamic and MHD theory to inhomogeneous flows, finding that the density fluctuations can also be of order Mach number, in agreement with a slightly different approach advocated by Bhattacharjee et al., 1998. The NI fluid models, unlike fully incompressible or compressible fluid descriptions, allow us to address weakly compressible effects directly in a quasi-neutral ISM fluid. Furthermore, NI theory has enjoyed notable success in describing fluctuations and turbulence in the supersonic solar wind. The NI model has recently been solved numerically and compared to observations in an effort to understand the Kolmogorov-like density spectrum in the ISM (Shaikh & Zank 2004, 2005, 2006, 2007, 2008, 2009, 2010). One of our results, shown in Fig 3, describes the evolution of density fluctuations from a fully compressible initial state. We find from our three-dimensional (decaying turbulence) simulations that a $k^{-5/3}$ density fluctuation spectrum emerges in fully developed compressible MHD turbulence from non-linear mode coupling interactions that lead to the migration of spectral energy in the transverse (i.e. $k \perp U$) Alfvenic fluctuations, while the longitudinal “compressional

modes” corresponding to $k \parallel U$ fluctuations make an insignificant contribution to the spectral transfer of inertial range turbulent energy. The explanation, in part, stems from the evolutionary characteristics of the MHD plasma that governs the evolution of the non-solenoidal velocity field in the momentum field. It is the non-solenoidal component of plasma motions that describes the high-frequency contribution corresponding to the acoustic time-scales in the modified pseudo-sound relationship (Montgomery et al. 1987; Matthaeus et al. 1998; Zank & Matthaeus 1990, 1993). What is notable in the work of Shaikh & Zank is that they find a self-consistent evolution of a Kolmogorov-like density fluctuation spectrum in MHD turbulence that results primarily from turbulent damping of non-solenoidal modes that constitute fast and slow propagating magnetoacoustic compressional perturbations. These are essentially a higher frequency (compared with the Alfvénic waves) component that evolve on acoustic timescales and can lead to a “pseudo-sound relationship” as identified in the nearly incompressible theory (Zank & Matthaeus 1990, 1993; Bayly et al. 1992; Matthaeus et al. 1998; Shaikh & Zank 2004a,b,c, 2006, 2007). The most significant point to emerge from the simulation is the diminishing of the high-frequency component that is related to the damping of compressible plasma motion. This further leads to the dissipation of the small-scale and high-frequency compressive turbulent modes. Consequently, the MHD plasma relaxes towards a nearly incompressible state where the density is convected passively by the velocity field and eventually develops a $k^{-5/3}$ spectrum. This physical picture suggests that a nearly incompressible state develops naturally from a compressive MHD magnetoplasma in the solar wind.

Among other work, describing a Kolmogorov-like $5/3$ spectrum in the context of MHD turbulence, are Cho & Vishniac (2000), Maron & Goldreich (2001), Cho, Lazarian & Vishniac (2002, 2003), Muller & Biskamp (2002), Cho & Lazarian (2002, 2003), Kritsuk et al. (2009). Our results, describing a Kolmogorov-like $5/3$ spectrum in the solar wind plasma, are thus consistent with these work. It is noted, however, that Maron & Goldreich (2001) report a Kraichnan-like $3/2$ spectrum in the inertial range for velocity fluctuations. The controversy of $5/3$ or $3/2$ is nonetheless beyond the scope of our review article.

1.5 Hall MHD model of SW turbulence- Extended spectra

To describe the extended solar wind spectra in Fig 2, time dependent, fully compressible three dimensional simulations of Hall MHD plasma in a triply periodic domain have been developed. This represents a local or regional volume of the solar wind plasma or ISP. The turbulent interactions in region II were described above by a 3D MHD model which is a subset of Hall MHD model since it does not contain the $\mathbf{J} \times \mathbf{B}$ term in the magnetic field induction equation. Note that the dynamics of length-scales associated with region III, i.e. corresponding to the KAW modes, cannot be described by the usual MHD models as they do not describe turbulent motions corresponding to the characteristic frequencies larger than an ion gyro fre-

quency. At 1 AU, ion inertial length scales are smaller than ion gyro radii in the solar wind (Goldstein 1995). Plasma effects due to finite Larmor radii can readily be incorporated in MHD models by introducing Hall terms to accommodate ion gyro scales up to scales as small as ion inertial length scales.

The Hall model in the limit of a zero ion-inertia converges to the usual MHD model, and assumes that the electrons are inertial-less, while the ions are inertial (Mahajan & Krishan 2004). Hence, the electrons and ions have a differential drift, unlike the one fluid MHD model for which the electron and ion flow velocities are identical. The Hall MHD description of magnetized plasma has previously been employed to investigate wave and turbulence processes in the context of solar wind plasma. Sahraoui et al. (2007) extended the ordinary MHD system to include spatial scales down to the ion skin depth or frequencies comparable to the ion gyrofrequency in an incompressible limit. They further analyzed the differences in the incompressible Hall MHD and MHD models within the frame work of linear modes, their dispersion and polarizations. Galtier (2006) developed a wave turbulence theory in the context of an incompressible Hall MHD system to examine the steepening of the magnetic fluctuation power law spectra in the solar wind plasma. Furthermore, Galtier & Buchlin (2007) have developed 3D dispersive Hall magneto-hydrodynamics simulations within the paradigm of a highly turbulent shell model and demonstrated that the large-scale magnetic fluctuations are characterized by a $k^{-5/3}$ -type spectrum that steepens at scales smaller than the ion inertial length d_i to $k^{-7/3}$. The observed spectral break point in the solar wind plasma, shown by the regime III in Fig 2, has been investigated using 3D simulations of a two fluid nonlinear Hall MHD plasma model (Shaikh & Zank, 2009).

In the inertial-less electron limit the electron fluid does not influence the momentum of solar wind plasma directly except through the current. Since the electron fluid contributes to the electric field, plasma currents and the magnetic field are affected by electron oscillations. The combination of electron dynamics and ion motions distinguishes the Hall MHD model from its single fluid MHD counterpart. Thanks to the inclusion of electron dynamics, Hall MHD can describe solar wind plasma fluctuations that are associated with a finite ion Larmor radius and thus a characteristic plasma frequency is $\omega > \omega_{ci}$. Because Hall MHD contains both ion and electron effects, there is a regime at which the one set of plasma fluctuations no longer dominates but instead is dominated by the other. This introduces an intrinsic scale length/timescale (frequency) that separates ion dominated behavior in the plasma from electron dominated. It is the Hall term corresponding to the $\mathbf{J} \times \mathbf{B}$ term in Faraday's equation that is primarily responsible for decoupling electron and ion motion on ion inertial length and ion cyclotron time scales (and introducing an intrinsic length scale). It is this feature that makes Hall MHD useful in describing dissipative solar wind processes when single fluid MHD is not applicable (the MHD model breaks down at $\omega > \omega_{ci}$). Hall MHD allows us to study inertial range cascades beyond $\omega > \omega_{ci}$, and can be extended to study dissipative heating processes where ion cyclotron waves are damped. However to study MHD processes, one can put $d_i = 0$ in region II. The extreme limit of fluid modeling applied to solar wind processes (even beyond the limit of the Hall MHD regime) is to use of an elec-

tron MHD model in which high frequency electron dynamics is treated by assuming stationary ions that act to neutralize the plasma background.

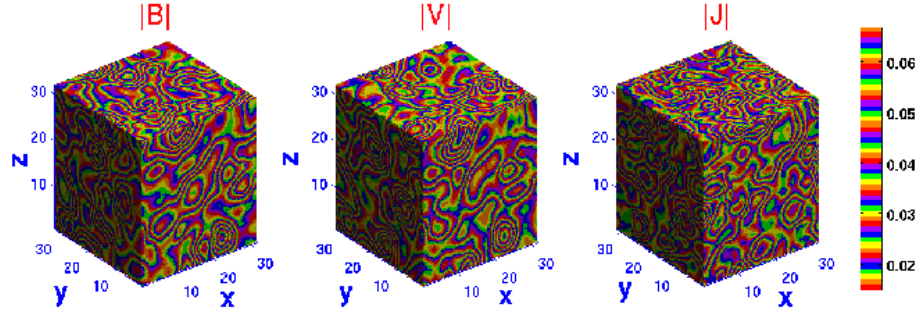


Fig. 4 Three dimensional structures of magnetic, velocity and current fields in Hall MHD turbulence. Turbulent equipartition between velocity and magnetic field leads to almost similar large scale structures in the two fields, while current is more intermittent.

Turbulence involves nonlinear interactions of modes in all three spatial directions. Three dimensional computations are numerically expensive, but, with the advent of high speed vector and parallel distributed memory clusters, and efficient numerical algorithms such as those designed for Message Passing Interface (MPI) libraries, it is now possible to perform magnetofluid turbulence studies at substantially higher resolutions. Based on MPI libraries, three dimensional, time dependent, compressible, non-adiabatic, driven and fully parallelized Hall magnetohydrodynamic (MHD) nonlinear codes have been developed that run efficiently on both distributed memory clusters like distributed-memory supercomputers or shared memory parallel computers. This allows for very high resolution in Fourier spectral space. Shaikh & Zank (2010) have developed a 3D periodic code that is scalable and transportable to different cluster machines, and extends earlier MHD codes of theirs (Shaikh & Zank ,2006, 2007, 2008, 2009, 2010). Their code treats the solar wind plasma fluctuations as statistically isotropic, locally anisotropic, homogeneous and random, consistent with ACE spacecraft measurements (Smith et al 2006). The numerical algorithm accurately preserve the ideal rugged invariants of fluid flows, unlike finite difference or finite volume methods. The conservation of ideal invariants (energy, enstrophy, magnetic potential, helicity) in inertial range turbulence is an extremely important feature because these quantities describe the cascade of energy in the inertial regime, where turbulence is, in principle, free from large-scale forcing as well as small scale dissipation. Damping of plasma fluctuations may nonetheless occur as a result of intrinsic non-ideal effects such those introduced by the finite Larmor radius. An example of the plasma velocity, magnetic field and current is shown in Fig 4.

In the simulations of Shaikh & Zank, the nonlinear spectral cascade in the modified KAW regime leads to a secondary inertial range in the vicinity of $kd_i \simeq 1$,

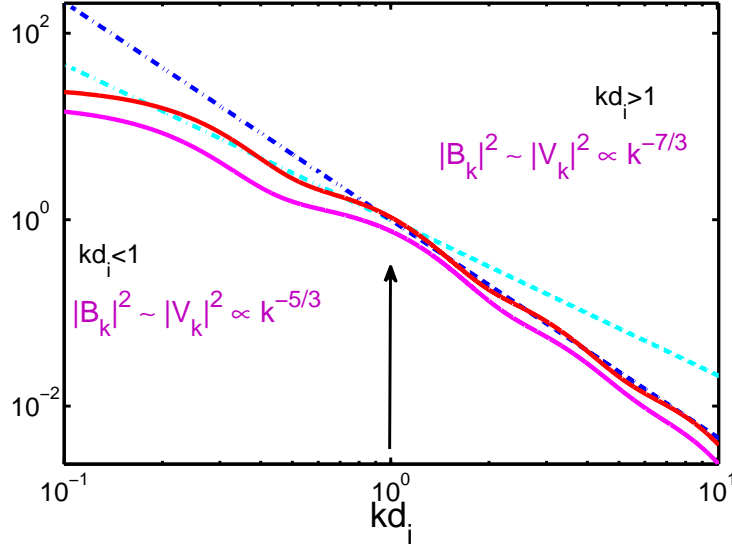


Fig. 5 Inertial range turbulent spectra for magnetic and velocity field fluctuations. The fluctuations closely follow respectively $k^{-5/3}$ and $k^{-7/3}$ scaling in the $kd_i < 1$ and $kd_i > 1$ KAW regimes. $kd_i = 0.05$ and 1.0 respectively in the $kd_i < 1$ and $kd_i > 1$ regimes. The dash-dot straight lines correspond to a $k^{-5/3}$ and $k^{-7/3}$ power law.

where the turbulent magnetic and velocity fluctuations form spectra close to $k^{-7/3}$. This is displayed in Fig 5, which also shows that for length scales larger than the ion thermal gyroradius, an MHD inertial range spectrum close to $k^{-5/3}$ is formed. The characteristic turbulent spectrum in the KAW regime is steeper than that of the MHD inertial range. Identifying the onset of the secondary inertial range has been the subject of debate because of the presence of multiple processes in the KAW regime that can mediate the spectral transfer of energy. These processes include, for instance, the dispersion and damping of EMICA waves, turbulent dissipation, etc.

Regimes IV and V, shown in the schematic of Fig 2, requires that we invoke a whistler model for the plasma. Whistler modes are excited in the solar wind plasma when the characteristic plasma fluctuations propagate along a mean or background magnetic field with frequency $\omega > \omega_{ci}$ and the length scales are $c/\omega_{pi} < \ell < c/\omega_{pe}$, where ω_{pi}, ω_{pe} are the plasma ion and pi pe electron frequencies respectively. The electron dynamics plays a critical role in determining the nonlinear interactions while the ions provide a stationary neutralizing background against fast moving electrons and behave as scattering centers. Whistler wave turbulence can be described by an electron magnetohydrodynamics (EMHD) model for the plasma (Kingsep et al 1990), utilizing a single fluid description of quasi neutral plasma. The EMHD model has been discussed in considerable detail in earlier work (Kingsep et al. 1990; Biskamp et al 1996; Shaikh et al. 2000a; Shaikh et al. 2000B; Shaikh &

Zank 2003; Shaikh & Zank 2005). In whistler modes, the currents carried by the electron fluid are important (Shaikh 2000, 2009, 2010). Turbulent interactions mediated by the coupling of whistler waves and inertial range fluctuations have been studied in three dimensions based on a nonlinear 3D whistler wave turbulence code (Shaikh & Zank, 2010).

Electron whistler fluid fluctuations, in the presence of a constant background magnetic field, evolve by virtue of nonlinear interactions in which larger eddies transfer their energy to smaller eddies through a forward cascade. The Kolmogorov model postulates that the cascade of spectral energy occurs exclusively between neighboring Fourier modes (i.e. local interaction) until the energy in the smallest turbulent eddies is finally dissipated. This leads to a damping of small scale motions. By contrast, the large-scales and the inertial range turbulent fluctuations remain unaffected by direct dissipation of the smaller scales. IN the absence of a mechanism to drive turbulence at the larger scales in the Shaikh & Zank 2009 simulations, the large-scale energy simply migrates towards the smaller scales by virtue of nonlinear cascades in the inertial range and is dissipated at the smallest turbulent length-scales. The spectral transfer of turbulent energy in the neighboring Fourier modes in whistler wave turbulence follows a Kolmogorov phenomenology (Kolmogorov 1941, Iroshnikov 1963, Kraichnan 1965) that leads to Kolmogorov-like energy spectra. Thus, the 3D simulations of whistler wave turbulence in the $kd_e < 1$ and $kd_e > 1$ regimes exhibits respectively $k^{-7/3}$ and $k^{-5/3}$ (see Fig 6) spectra. The inertial range turbulent spectra obtained from 3D simulations are consistent with 2D models (Shaikh & Zank 2005). The whistler wave dispersion relation shows that wave effects dominate at the large scale, i.e. the $kd_e < 1$ regime, and the inertial range turbulent spectrum exhibits a Kolmogorov-like $k^{-7/3}$ spectrum. On the other hand, turbulent fluctuations on smaller scales (i.e., in the $kd_e > 1$ regime) behave like non-magnetic eddies in a hydrodynamic fluid and yield a $k^{-5/3}$ spectrum. The wave effect is weak, or negligibly small, in the latter. Hence the nonlinear cascades are determined essentially by the hydrodynamic-like interactions. Thus, the observed whistler wave turbulence spectra in the $kd_e < 1$ and $kd_e > 1$ regimes (Figs 6) can be understood on the basis of Kolmogorov-like arguments that describe the inertial range spectral cascades. In the electron whistler wave regime, the fluid simulations describing a $7/3$ spectrum are also reported by Ng et al. (2003), Cho & Lazarian (2004, 2010). Their results are consistent with our simulations described in Fig (6a).

We note that $7/3$ regime of whistler turbulence is different from the usual $5/3$ regime in the MHD turbulence. The $5/3$ regime does not terminate sharply beyond the inertial range MHD fluctuations, but there is another cascade regime, not describable by the MHD equations, that deviates significantly from the $5/3$ regime and is describable by whistler mode turbulence.

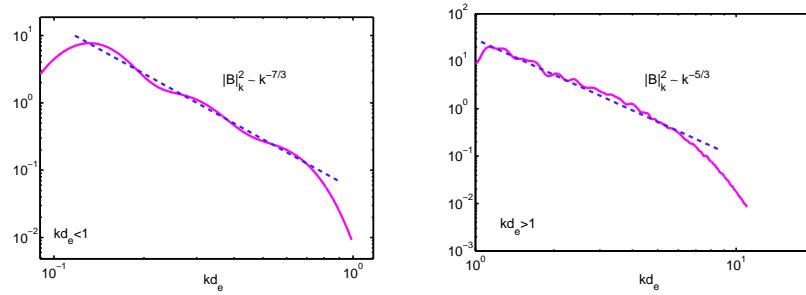


Fig. 6 (Left) 3D simulation of whistler wave turbulence in the $kd_e < 1$ regime exhibits a Kolmogorov-like inertial range power spectrum close to $k^{-7/3}$. (Right) The small scales magnetic field fluctuations in the $kd_e > 1$ regime depicts a Kolmogorov-like $k^{-5/3}$ spectrum which is a characteristic of hydrodynamic fluid.

2 Perpendicular shocks

Diffusive shock acceleration (DSA) is considered to be the mechanism responsible for the acceleration of energetic particles and the consequent generation of power-law spectra observed at quasi-parallel shocks (Axford et al., 1977; Bell 1978; Blandford & Ostriker, 1978). At a quasi-parallel shock, energetic ions can be scattered by the self-excited and pre-existing waves and turbulence upstream and downstream of the shock, so leading to their multiple crossing of the shock. Because these ions can stream far upstream along the magnetic field and excite low-frequency plasma waves, the turbulence responsible for particle scattering ahead of the shock is present. In this way, energetic particles can be accelerated by DSA to high energies and form a power-law spectrum (Lee, 1983; Zank et al, 2000).

At a quasi-perpendicular shock, no self-consistent plasma wave excitation occurs upstream, which therefore limits particle scattering. Because of this, DSA cannot be used to explain the observed power-law spectra of energetic particles at quasi-perpendicular shock waves in the usual way. Lu et al. (2009) investigated the interaction of Alfvén waves with a perpendicular shock using a two-dimensional hybrid simulation. Alfvén waves are injected from the left boundary, and they have no obvious effects on the propagation speed of the shock. After the upstream Alfvén waves are transmitted into the downstream, their amplitude is enhanced by about 10-30 times. Consistent with the fluid theory (McKenzie & Westphal, 1969), the transmitted waves can be separated into two parts: one that propagates along the direction parallel to the background magnetic field, and the other along the direction anti-parallel to the background magnetic field. In addition, we also find obvious ripples in the shock front due to the interaction of the Alfvén waves and the perpendicular shock.

In a realistic shock, of course, the structure of a quasi-perpendicular shock is considerably more complicated than described above, and the meandering magnetic field lines can cross the shock front more than once. Kóta (2009) has discussed the

efficiency of ion acceleration at a perpendicular shock using an analytical approximation and numerical simulations. Energetic ions are generated at places where the field lines cross into the upstream region and soon re-cross the shock back to the downstream region. These ions may be accelerated to very high energies through multiple mirroring at the stronger downstream field.

Umeda et al. (2009) also discussed the effect of the rippling of perpendicular shock fronts on electron acceleration in the shock-rest-frame using a full particle simulation. The cross-scale coupling between ion-scale mesoscopic shock ripples and an electron-scale microscopic instability was found to play an important role in energizing electrons at quasi-perpendicular shocks. At the shock front, the ions reflected by the shock experience considerable acceleration upstream at a localized region where the shock-normal electric field of the rippled structure is polarized upstream. The current-driven instability is unstable and large-amplitude electrostatic waves grow upstream. As a result, electrostatic waves can trap electrons upstream, and then energetic electrons are generated via a form of surfing acceleration at the leading edge of the shock transition region.

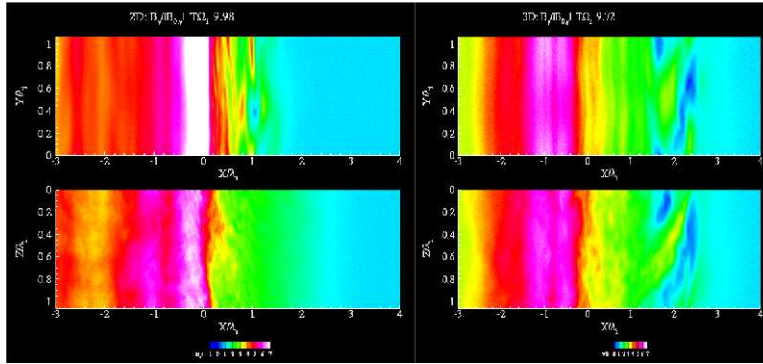


Fig. 7 Color contours of the B_y component (the major component of the magnetic field), showing (a) two 2D results (in the XY and XZ planes), and (b) a 3D result. The 3D results show that large amplitude wave active exists persistently (independent of the reformation phase) in the furthest front of the shock. [Shinohara and Fujimoto (2009).]

Shinohara & Fujimoto (2009) discussed non-stationary behavior of the shock front, since it has been thought to play an important role for dissipation mechanism in collision-less shocks. Using JAXA's new super-computer facility allowed them to perform a three-dimensional simulation of a quasi-perpendicular shock. The simulation parameters were selected to simulate specific Cluster observational results. The full ion to electron mass ratio, $M/m = 1840$, was used, and almost (one ion inertia length)² square plane perpendicular to the upstream flow direction was allocated for this simulation. The 3D results of Shinohara & Fujimoto (2009) showed that both self-reformation and whistler emission are present. By comparing their 3D results with 2D simulations based on the same simulation parameters (Fig. 7), they confirmed that the 3D result is not simply a superposition of 2D behavior but

instead identified new wave activity in the front of the shock foot region. Because of the enhanced wave activity, electrons are much more efficiently heated in the 3D simulations than in 2D simulations. That the shock structure is changed significantly in adding a further degree of freedom with the third spatial dimension emphasizes the importance of fully multi-dimensional studies. The simulation of Shinohara & Fujimoto (2009) also identifies the importance of using the full mass ratio in simulations.

3 Global magnetospheric modeling and observations

A systematic evaluation of ground and geostationary magnetic field predictions generated by a set of global MHD models shows that a metrics analysis of two different geospace parameters, the geostationary and ground magnetic field, yields surprising similarities. However, the parameters reflect rather different properties of geospace (Pulkkinen et al., 2010). More specifically, by increasing the spatial resolution and including more realistic inner magnetospheric physics made the model predictions by the BATS-R-US model more accurate. By contrast, the OpenGGCM model had a tendency to generate larger differences to observations than BATS-R-US in terms of the prediction efficiency, but the model provided more accurate representation of the observed spectral characteristics of the ground and geostationary magnetic field fluctuations. This suggests that both models capture some of the intrinsic physical elements necessary to realistic modeling, but the complexity of identifying realistic boundary conditions and the capturing of the physics between different plasma regimes in the Earth-magnetospheric interaction means that this will remain an outstanding problem for years to come.

It is well known that the southward component of the interplanetary magnetic field (IMF) B_z is the primary heliospheric parameter responsible for geomagnetic storms. Yakovchouk et al. (2009) performed a statistical analysis of the peak values of the IMF B_z component with different combinations of plasma parameters and the hourly Dst (omniweb.gsfc.nasa.gov) and Dxt/Dcx (Karinen and Mursula, 2005, 2006) geomagnetic indices for all identified perturbations in 1963- 2009 (Fig. 8a). Storms without available interplanetary data were not included in the database. Yakovchouk et al. (2009) concluded that the storms occur more often (twice as often) during the development phase of the solar cycle than during the rising phase. The average waiting time between consecutive Dst peaks is 11 days for $Dst \geq -50$ nT and 50 days for $Dst < -100$ nT. The average delay time between Dst and B_z peak values is 4-6 hours. A semiannual variation of the Dst peak values exists for all levels. Empirical formulae are derived by Yakovchouk et al. (2009) that relate $Dst/Dcx/Dxt < -50$ nT and B_z/E_y values ($E_y = U_x B_z$ - the peak value of electric field, where U_x is the radial velocity component of the solar wind) based on their analysis of the observations. The relations that they present are in a good agreement with the Akasofu relation (Akasofu, 1981), and are useful for quick estimates and reconstruction of heliospheric and geomagnetic parameters with accuracy of the or-

der of a few tens percent (Fig. 8a). A dependence of the area for the development phase duration of storms with Dst and Bz peaks also exists (Fig. 8b). The accuracy of reconstruction is less when only fragmentary geomagnetic data are available.

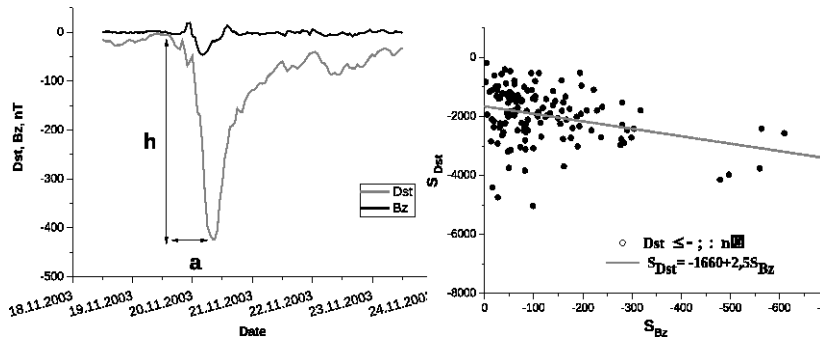


Fig. 8 (a) An example of a large geomagnetic storm showing the Bz and Dst profiles as a function of time. (b) The dependence of area ($S=h \times a$) for the development phase duration of a storm for Dst and Bz peaks in 1963-2009 and its approximation by a linear fit. (Yakovchouk et al., 2009.)

4 Distribution functions of protons and interstellar hydrogen in the inner and outer heliosheath

The Interstellar Boundary EXplorer (IBEX) (McComas et al., 2006, McComas et al., 2009), launched on 19 October, 2008, is measuring the energetic neutral atom (ENA) flux from the boundary regions of our heliosphere. Contemporaneously, Voyager 1 and 2 (V1, V2) are making in situ measurements of plasma, energetic particles, and magnetic fields along two trajectories in the heliosheath (Stone et al., 2008, Richardson et al., 2008, Decker et al., 2008, Burlaga et al., 2008, Gurnett et al., 2008). The interpretation of the IBEX observations will depend critically on global simulations of the solar wind-local interstellar medium (LISM) interaction e.g., Heerikhuisen et al., 2008, informed by in situ data returned by the Voyager spacecraft. Underlying the determination of the ENA flux observed at 1 AU is the form of the proton distribution function in the inner and outer heliosheath. ENAs are created by charge exchange of interstellar neutral H and heliosheath (inner and outer) protons or ions. Because the inner heliosheath is hot, a population of energetic neutral atoms is created. The flux of ENAs will therefore depend quite sensitively on the number of particles in the wings of the hot proton population downstream of the heliospheric termination shock (TS), something recognized by both Prested et al., 2008 and Heerikhuisen et al., 2008 in their introduction of a κ -distribution to model the inner heliosheath proton distribution. In particular, in an important extension of their earlier work, Heerikhuisen et al., 2008 developed a fully self-consistent

3D MHD-kinetic neutral hydrogen (H) model describing the solar wind-LISM interaction (Pogorelov et al., 2006, Pogorelov et al., 2007, Pogorelov et al., 2008) using a κ -distribution to describe the underlying proton distribution in the inner heliosheath. Previous models assumed a Maxwellian description for the protons with self-consistent coupling to interstellar neutral H – the self-consistent coupling being crucial in determining the global heliospheric structure (Baranov & Malama, 1993, Pauls & Zank, 1995, Zank et al., 1996a, Pogorelov et al., 2006) (see Zank 1999, Zank et al., 2009 and Pogorelov et al., 2009 for extensive reviews). Prested et al., 2008 by contrast used a test particle approach to model the neutral H production based on an ideal MHD model.

The treatment of the heliospheric proton distribution function as a κ -distribution yields important differences in both the global structure of the heliosphere (decreasing the overall extent of the inner heliosheath between the TS and the heliopause) and the predicted ENA flux at 1 AU (Heerikhuisen et al., 2008). By assuming a κ -distribution with index $\kappa = 1.63$ (this motivated by the observed spectral index associated with energetic particles downstream of the heliospheric termination shock, Decker et al., 2005), Heerikhuisen et al. 2008 find that the ENA flux at 1 AU is substantially higher than for a corresponding Maxwellian proton distribution with the same temperature. This is not especially surprising of course because the κ -distribution contains many more particles in the wings of the distribution than the corresponding Maxwellian, thereby giving higher fluxes of ENAs at higher energies. Why the heliosheath proton distribution function should be like a kappa distribution with a spectral index close to 1.63 is however quite unclear. The answer may well reside in the processing of the upstream pickup ion distribution by the TS and the subsequent statistical relaxation of the processed distribution in the heliosheath (Livadiotis & McComas, 2009). IBEX will provide definitive observations of the ENA flux at 1 AU that will allow us to estimate the proton distribution in the inner heliosheath.

Related to the question of the heliosheath proton distribution are the plasma and magnetic field observations made by Voyager 2 on the second crossing of the TS. V2 has a working plasma instrument and the coverage was sufficient to identify three distinct crossings of the TS and make in situ measurements of the microstructure. The identified TS-3 crossing revealed an almost classical perpendicular shock structure (Burlaga et al., 2008, Richardson et al., 2008). However, plasma measurements revealed that the solar wind proton temperature changed from 20,000 K upstream to 180,000 K downstream (Richardson et al., 2008, Richardson, 2009). Although hot solar wind plasma is sometimes observed, the average downstream proton plasma temperature is an order of magnitude smaller than predicted by the MHD Rankine-Hugoniot conditions, and the global self-consistent models all yield downstream proton temperatures of $\sim 2 \times 10^6$ K (Zank et al. 2009). The downstream shock heated solar wind ion temperature observed by V2 is in fact so low that the downstream flow appears to remain supersonic (Richardson et al., 2008)! Furthermore, the transmitted solar wind proton distribution appears to be essentially a broadened/heated Maxwellian (with a somewhat flattened peak), and there is no evidence of reflected solar wind ions being transmitted downstream (Richard-

son, 2009). Richardson et al. 2008 and Richardson 2009 concluded that pickup ions (PUIs) experienced preferential heating at the TS and thus provided both the primary shock dissipation mechanism and the bulk of the hot plasma downstream of the TS. Unfortunately, the Voyager spacecraft were not instrumented to measure PUIs directly. That PUIs provide the TS dissipation and heated downstream plasma had in fact been predicted by Zank et al. 1996b in their investigation of the interaction of PUIs and solar wind ions with the TS. They concluded that “P[U]Is may therefore provide the primary dissipation mechanism for a perpendicular TS with solar wind ions playing very much a secondary role.” Thus the basic model of Zank et al. 1996b for the microstructure of the TS appears to be supported by the V2 observations. However, both the observed solar wind proton distribution and a shock dissipation mechanism based on PUIs means that the downstream proton distribution function is a (possibly complicated) function of the physics of the TS. Zank et al., 2010 have extended their basic model of the quasi-perpendicular TS, mediated by PUIs, to derive the complete downstream proton distribution function in these regions, identifying the partitioning of energy between solar wind protons and PUIs, and inferred potential implications of these results for the ENA flux observed at 1 AU in terms of spectra and skymaps. They did not attempt to synthesize a complete description of the inner heliosheath proton distribution at this point, preferring instead to elucidate the physics of the quasi-perpendicular termination shock, and relate that physics to the production of ENAs. Other regions of the TS, notably the high polar regime and possibly the heliotail region of the TS, may require the introduction of distinctly different physical processes for shock dissipation, and a complete model of the heliosheath proton distribution will therefore need to account for multiple shock regimes. Katushkina & Izmodenov 2009 have begun to explore different aspects of this.

The model developed by Zank et al., 2010 describes the basic plasma kinetic processes and microphysics of the quasi-perpendicular TS in the presence of an energetic PUI population. They find that the solar wind protons do not experience reflection at the cross-shock potential of the TS, and are transmitted directly into the heliosheath. PUIs, by contrast, can be either transmitted or reflected at the TS, and provide the primary dissipation mechanism at the shock, and dominate the downstream temperature distribution. An inner heliosheath proton distribution function was derived that is 1) consistent with V2 solar wind plasma observations, and 2) is similar to a κ -distribution with index 1.63. The composite inner heliosheath proton distribution function is a superposition of cold transmitted solar wind protons, a hot transmitted PUI population, and a very hot PUI population that was reflected by the cross-shock electrostatic potential at least once before being transmitted downstream. The composite spectrum possesses more structure than the κ -distribution but both distributions have approximately the same number of protons in the wings of the distribution (and therefore many more than a corresponding Maxwellian distribution). Finally, ENA spectra from various directions at 1 AU generated by either the composite (TS) heliosheath proton distribution or the κ -distribution are very similar in intensity, although some structure is present in the composite case. The spectral shape is a consequence of the contribution to the ENA flux by primarily

heliosheath transmitted and reflected PUIs. The ENA spectrum is dominated by transmitted PUI created ENAs in the energy range below 2 keV and reflected PUI created ENAs in the range above 2 keV. This may give us an opportunity to use IBEX data to directly probe the microphysics of the TS. The skymaps are dominated by ENAs created by either transmitted PUIs or reflected PUIs, depending on the energy range.

IBEX, in completing its first full scan of the sky, created maps of energetic neutral atom (ENA) flux for energies between 100 eV and 6 keV (McComas et al. 2009a; Schwadron et al. 2009; Funsten et al. 2009b; Fuselier et al. 2009). The overall flux intensities appear to be generally within about a factor of two or three of those predicted by global models of the interaction between the solar wind (SW) and local interstellar medium (LISM). A most unexpected feature was the presence in the IBEX ENA maps of a “ribbon” that encircles the sky, passing closer to the heliospheric nose direction in the south and west than in the north and east. The ribbon represents a nearly threefold enhancement in ENA flux compared to adjacent parts of the sky, but the shape and magnitude of the energy spectrum is primarily ordered by ecliptic latitude rather than its location inside or outside of the ribbon (Funsten et al. 2009b). This suggests that ENAs inside the ribbon come from the same population of parent ions. 3D global heliospheric models make it possible to simulate the flux of ENAs at 1 AU (Fahr & Lay 2000; Gruntman et al. 2001; Heerikhuisen et al. 2007; Sternal et al. 2008; Prested et al. 2008; Heerikhuisen et al. 2008; Izmodenov et al. 2009). The assumptions made by global models have been refined as new observational data emerged. For example, the termination shock (TS) crossing by the Voyager 1 & 2 spacecraft, in 2004 and 2007 respectively (Stone et al. 2005, 2008), suggested a north-south asymmetry of the heliosphere. The inferred asymmetry led to new global models with larger than previously thought interstellar magnetic field (ISMF) strengths (Pogorelov et al. 2007, 2009; Izmodenov et al. 2009). Measurements of Lyman-alpha back-scattered photons in the nearby SW (Lallement et al. 2005), suggest asymmetries in the outer heliosheath (OHS) that can be linked to the plane of the LISM magnetic and velocity vectors – the so-called “hydrogen deflection plane”. Models confirmed (Izmodenov et al. 2005; Pogorelov et al. 2008, 2009) that the deflection of interstellar hydrogen from helium due to the shape of the OHS does indeed take place primarily in the hydrogen deflection plane. The IBEX observations enable the first global validation of these models and their components and, thus, yield insight into the physical processes that drive the structure and dynamics of the outer heliosphere. The fact that the ribbon was not predicted by any models suggests that it is generated by physical processes that have so far been omitted from models.

The relationship between the ribbon and the region just outside the heliopause where the ISMF is perpendicular to radial vectors from the sun, was discovered by the IBEX team (McComas et al. 2009a; Funsten et al. 2009b; Schwadron et al. 2009) using model results from Pogorelov et al. (2009). Several possible explanations for this correlation were given in those papers, some of which rely on stresses created by the ISMF near the heliopause to generate regions of enhanced density which, combined with a local population of non-isotropic PUIs, may lead to enhanced ENA

emissions. However, plots of the total pressure (magnetic plus thermal) on the surface of the simulated heliopause display no banded structures related to magnetic forces or density enhancements at all. Self-consistently coupled MHD-neutral solution indicate that enhancements in magnetic pressure and thermal pressure are somewhat anti-correlated, resulting in a relatively smooth total pressure profile. The underlying physics for generating the ribbon discovered in the IBEX data must explain a number of observed features. Firstly, the ribbon appears to be closely related to the orientation of the magnetic field just outside the heliopause, in a way that links enhanced ENA flux to regions where the outer heliosheath magnetic field \mathbf{B}_{OHS} is perpendicular to the heliocentric radial vector \mathbf{r} (see figure 4 in McComas et al. (2009a); figure 3 in Funsten et al. (2009b); and figure 2 in Schwadron et al. (2009)) such that $\mathbf{B}_{\text{OHS}} \cdot \mathbf{r} \sim 0$. Secondly, it needs to explain why the spectrum of ENAs is very nearly the same inside and outside the ribbon (figure 2 in McComas et al. (2009a)). Thirdly, it must be based on physical processes that are excluded from all previous heliospheric models, thereby explaining why no ENA ribbon feature has been seen in any models of the SW-LISM interaction.

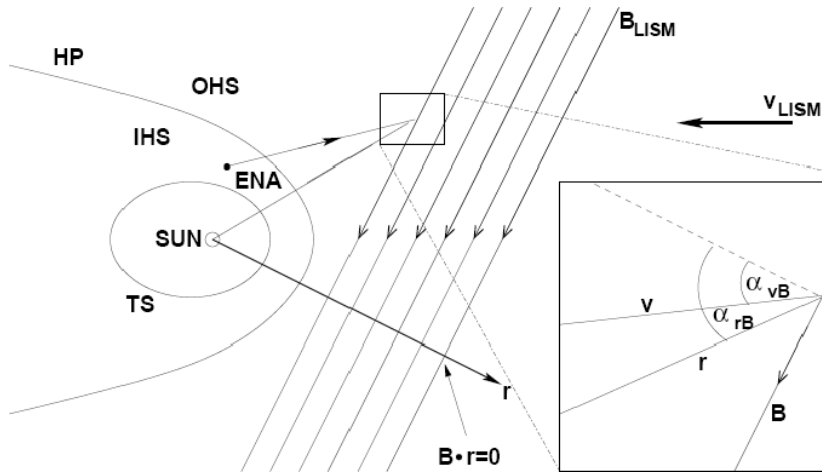


Fig. 9 Schematic of the heliosphere in the plane containing the ISMF and velocity vectors (\mathbf{B}_{LISM} & \mathbf{v}_{LISM}). A primary energetic neutral atom (ENA) created in the inner heliosheath (IHS) region between the termination shock (TS) and the heliopause (HP) is shown as it moves into the outer heliosheath (OHS) whereupon it ionizes and becomes an outer heliosheath pickup ion (PUI) that can re-neutralize to form a secondary ENA. Note that the OHS magnetic field becomes highly warped close to the heliopause (see Pogorelov et al., 2009). [Heerikhuisen et al., 2010]

Heerikhuisen et al., 2010 considered the possibility that solar wind-created neutrals could create pick-up ions (PUIs) in the outer heliosheath to explain the ribbon of enhanced ENA flux observed by IBEX. Their approach relies on the fact that the average velocity of ions in the SW and inner heliosheath (IHS) is anti-sunward, so that the majority of ENAs propagate away from the sun into the outer heliosheath. In the region of enhanced interstellar plasma density surrounding the heliopause, some

of these ENAs charge-exchange and create PUIs in the slow warm subsonic plasma of the outer heliosheath. These PUIs will initially form a ring-beam distribution, with a velocity component along the magnetic field. Over time this distribution will isotropize by wave-particle interactions (Williams & Zank 1994). However, the ring distributed PUIs may charge-exchange with the fairly dense interstellar hydrogen ($> 0.2 \text{ cm}^{-3}$), resulting in a new “secondary” ENA. These secondary ENAs have been included in models before (Izmodenov et al. 2009), but only in an isotropic way for an axially symmetric heliosphere without an interstellar magnetic field (ISMF). If “re-neutralization” occurs quickly, the PUI will not have had time to scatter to some random direction over a complete shell, but rather the secondary ENA will be directed to some random vector on a partial shell. Furthermore, in locations where $\mathbf{B}_{\text{OHS}} \cdot \mathbf{r} \sim 0$, the plane of the ring about which the shell distribution is forming intersects the Sun, and leads to an increased ENA flux from these locations (see Fig 9). This mechanism could thus explain the link between the ribbon and the orientation of the ISMF.

Heerikhuisen et al., 2010 used a 3D steady-state MHD-plasma/kinetic neutral model of the heliosphere (Heerikhuisen et al. 2008, 2009; Pogorelov et al. 2008), with uniform SW conditions and a 3 G ISMF in the hydrogen deflection plane pointed towards ecliptic coordinate (224,41). The LISM boundary conditions are consistent with the analysis of Slavin & Frisch (2008). They used a Lorentzian (or “kappa”) distribution for IHS protons. Plotted in Figure 10 are all-sky maps of ENA flux for both the simulated and observed data. The simulated ribbon does not line up exactly, but the offset is almost certainly due to a slightly “incorrect” choice of the ISMF orientation in the simulation. The observed ribbon, particularly the southernmost portion, moves slightly at high energies. The Heerikhuisen et al. simulation reproduces this effect, which can be attributed to the larger mean free path of high energy primary ENAs resulting in a ribbon from PUIs at a larger distance into the outer heliosheath, where the magnetic field orientation is slightly different.

A second important observation is the absence of a unique spectral signature associated with the ribbon. The all-sky spectrum predicted by the Heerikhuisen et al simulations shows that the ribbon appears to have a locally steeper spectrum, while the observed spectrum shows almost no change across the ribbon. One reason for a steeper ribbon spectrum in the simulation is that a “bump” is formed at the SW energy, which is uniform and constant in their simulation while in reality the bump should be spread over a time-averaged SW energy profile. This deficiency may be addressed in future models by using a spectrum that depends on physical processes of energization at the termination shock as experienced by core SW ions and PUIs (Zank et al. 2010). Using such a composite spectrum would also allow for spectral indices of less than 1.5 over the IBEX energy range, something that is not possible with a κ -distribution (Livadiotis & McComas 2009).

Finally, A careful comparison with the observed ribbon suggests that if the Heerikhuisen mechanism is correct, then the ISMF is directed close to the ecliptic coordinates (224,41) used in their model, and close to the value (221,39) corresponding to the center of the ribbon observed in Funsten et al. (2009b).

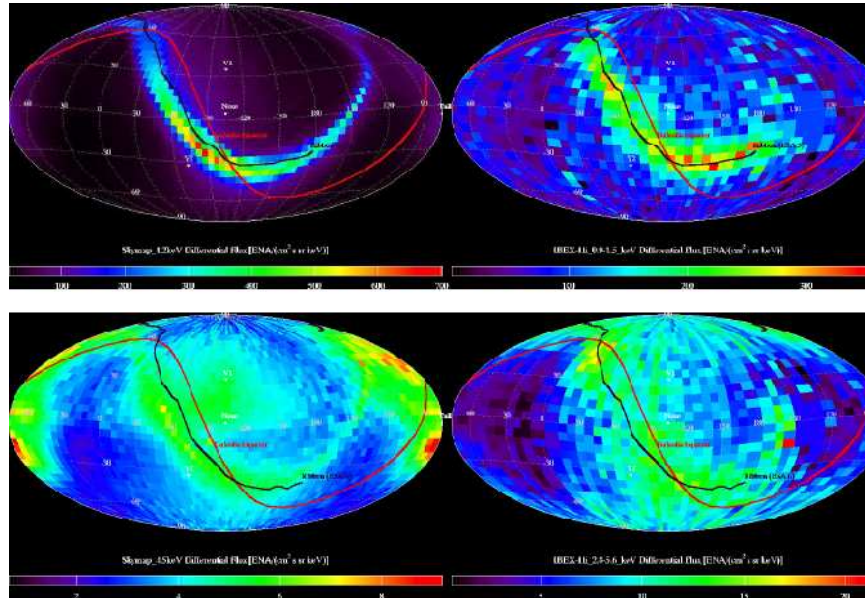


Fig. 10 All-sky maps of simulated (left) and observed (right) ENA flux at 1.1 keV (top) and 4.5 keV (bottom). The simulation uses a $\alpha = 1.63$ spectral index for IHS protons and has assumed that all PUIs retain partial shell distributions long enough to re-neutralize before they isotropize. The red curve is the galactic plane, and a best fit to the observed ribbon is shown as a black line. Note that the ribbon shifts down slightly at high energies. Units of ENA flux are $(\text{cm}^2 \text{ s sr keV})^{-1}$. [Heerikhuisen et al., 2010]

5 Conclusions

We have considered several illustrative examples of the complicated interplay and coupling between large and small space-time scales, and slow and fast processes in space plasmas of magnetospheric, heliospheric and interstellar origin. Laminar and turbulent processes coexist, and energy transfer manifests itself from small to large and large to small scales - essentially direct and inverse cascades - ensuring that a full understanding of complex space plasma systems requires the proper coupling of disparate scales.

Acknowledgements Acknowledgements This study was fulfilled as a part of the Programs of the Russian Academy of Sciences: “Origin and Evolution of Stars and Galaxies” (P-04), “Solar Activity and Space Weather” (P-16, Part 3) and Plasma Processes in the Solar System (OFN-15), MSU Interdisciplinary Scientific Project and supported by the RFBR grants 07-02-00147, NSh-1255.2008.2. DS and GPZ acknowledge the partial support of NASA grants NNX09AB40G, NNX07AH18G, NNG05EC85C, NNX09AG63G, NNX08AJ21G, NNX09AB24G, NNX09AG29G, and NNX09AG62G. The authors are grateful to participants of the IAGA meeting in Sopron who provided their published materials used for the preparation of this paper.

References

1. Alexandrova, O.; Carbone, V.; Veltri, P.; Sorriso-Valvo, L. 2007, *Planet. Space Sci.* 55, 2224.
2. Alexandrova, O.; Carbone, V.; Veltri, P.; Sorriso-Valvo, L. 2008, *Astrophys. J.* 674, 1153.
3. Armstrong J. W., Cordes J. M., Rickett B. J., 1981, *Nat*, 291, 561.
4. Armstrong, J. W., Rickett, B. J., & Spangler, S. R. 1995, *ApJ*, 443, 209.
5. Armstrong J. W., Coles W. A., Kojima M., Rickett B. J., 1990, *Astrophys. J.*, 358,685.
6. Axford, W. I., E. Leer, & G. Skadron (1977), in *Proc. 15th Int. Conf. on Cosmic Rays*, Vol. 11, ed. C. Ya. Christou (Sofia: Bulgarian Acad. Sci.), 13.
7. Bale, S., et al. 2005, *Phys. Rev. Lett.*, Vol. 94, 215002.
8. Baranov V.B. & Yu.G.Malama, 1993, *J. Geophys. Res.*, Vol. 98, 15157-15163.
9. Bayly, B. J., Levermore, C. D., and Passot, T., 1992, *Phys. Fluids*, A 4, 945954.
10. Beinroth, H. J., and Neubauer, F. M. 1981, *J. Geophys. Res.*, Vol. 86, 7755.
11. Bell A. R. 1978, *MNRAS*, Vol. 182, 147-156.
12. Beresnyak, A., Lazarian, A., & Cho, J. 2005, *ApJL*, 624, L93.
13. Biskamp, D., *Magnetohydrodynamic Turbulence*, Published by Cambridge University Press, 2003.
14. Biskamp, D., Schwarz, E., and Drake, J. F. 1996, *Phy. Rev. Lett.*, 76, 1264.
15. Bhattacharjee, A., C. S. Ng, and S. R. Spangler, 1998, *Astrophys. J.*,494, 409.
16. Blandford, R. D. & J. P. Ostriker, 1978, *Astrophys. J.*, Vol. 221, L29-L32.
17. Brandt P.C., E.C. Roelof, P. Wurz, S. Barabash, D. Bazell, R. DeMajistre, T. Sotirelis & R. Decker (2009), *Geophysical Research Abstracts*, vol. 11, EGU2009-9588.
18. Bruno R. & V.Carbone (2005), *Living Rev. Solar Phys.* 2, 4. URL (cited on ;25.07.2009;): <http://www.livingreviews.org/lrsp-2005-4>.
19. Burlaga, L.F., et al., 2008, *Nature*, 454, 75.
20. Chepurinov, A., & Lazarian, A. 2010, *ApJ*, 710, 853.
21. Cho, J., & Lazarian, A. 2002, *Physical Review Letters*, 88, 245001.
22. Cho, J., & Lazarian, A. 2003, *MNRAS*, 345, 325.
23. Cho, J., & Lazarian, A. 2009, *ApJ*, 701, 236.
24. Cho, J., Lazarian, A., & Vishniac, E. T. 2002, *ApJ*, 564, 291.
25. Cho, J., Lazarian, A., & Vishniac, E. T. 2003, *ApJ*, 595, 812.
26. Cho, J., & Vishniac, E. T. 2000, *ApJ*, 539, 273.
27. Decker, R.B. et al., 2005, *Science*, 309, 2020.
28. Decker, R.B. et al., 2008, *Nature*, 454, 67.
29. Denskat, K. U., and Neubauer, F. M. 1982, *J. Geophys. Res.*, Vol. 87, 2215.
30. Elmegreen, B. G., & Scalo, J. 2004, *ARAA*, 42, 211.
31. Frisch U. 1995, *Turbulence: The Legacy of A. N. Kolmogorov*. Cambridge University Press.
32. Fuselier S. A. et al. (2009), *Science*, 326, 5955, 962-964. DOI: 10.1126/science.1180981.
33. Funsten, H., et al., 2009, *Science*, 1, 10, 1126.
34. Galtier, S. 2008, *J. Geophys. Res.*, 113, A01102, doi:10.1029/2007JA012821.
35. Galtier, S., 2006, *J. Plasma Phys.*, Vol. 72, 721.
36. Galtier, S. and Buchlin, E. , 2007, *Astrophys. J.*, Vol. 656, 560.
37. Gary, S. P., et al., 2008, *Geophys. Res. Lett.* 35, L02104.
38. Ghosh, S. Siregar, E., Roberts, D. A. and Goldstein, M. L., 1996, *J. Geophys. Res.*, 101, 2493.
39. Ghosh, S. and Goldstein, M. L., *J. Plasma Phys.* 1997, 57, 129.
40. Goldstein,M.L.; Roberts,D.A.; Matthaues,W.H. 1995, *Annual Review of Astronomy and Astrophysics*, 33, 283.
41. Goldstein, M. L.; Roberts, D. A.; Fitch, C. A., 1994, *J. Geophys. Res.*, Vol. 99, 11,519.
42. Gurnett, D. A. and Kurth, W.S., 2008, *Nature*, 454, 67.
43. Hasegawa, A., and Chen, L. 1976, *Phys. Rev. Lett.*, 36, 1362.
44. Heerikhuisen, J., V. Florinski, & G.P. Zank, 2006, *J. Geophys. Res.*, 111, A06110.
45. Heerikhuisen, J., N.V. Pogorelov, V. Florinski, G.P. Zank, J. le Roux, 2008, *Astrophys. J.*, 682, 679.

46. Heerikhuisen, J., N.V. Pogorelov, G.P. Zank, G.B. Crew, P.C. Frisch, H.O. Funsten, P.H. Janzen, D.J. 2010, *Astrophys. J.*, 708L, 126.
47. Higdon J. C., 1984, *Astrophys. J.*, 285, 109.
48. Higdon J. C., 1986, *Astrophys. J.*, 309, 342.
49. Howes, G. G., Dorland, W., Cowley, S. C., Hammett, G. W., Quataert, E., Schekochihin, A. A., and Tatsuno, T., 2008, *Phys. Rev. Lett.* 100, 065004.
50. Hunana, P., Zank, G.P., and Shaikh, D., 2006, *Phys. Rev. E*, vol. 74, 2, 026302.
51. Hunana, P. & G.P. Zank, Inhomogeneous nearly incompressible description of magnetohydrodynamic turbulence, *Phys. Fluids*, submitted, 2010.
52. Iroshnikov P. S., 1963, *Astron. Zh.*, 40, 742.
53. Iroshnikov P.S. 1963, *Sov. Astron.*, 7, 4. 566-571.
54. Izmodenov V.V., Y.G.Malama, M.S.Ruderman, S.V.Chalov, D.B.Alexashov, O.A.Katushkina & E.A.Provornikova (2009), *Space Sci. Rev.*, 146, 329-351.
55. Izmodenov, V., Alexashov, D., & Myasnikov, A. 2005, *A & A*, 437, L35.
56. Karinen A. & K. Mursula, 2006, *J. Geophys. Res.*, Vol. 111, A8, CiteID A08207.
57. Katushkina O. & V. Izmodenov (2009), Paper 402-TUE-01145-0862 presented at the IAGA 11th Scientific Assembly, August 23-30, 2009, Sopron, Hungary, Programme, p.51.
58. Kolmogorov A. N., 1941, *Dokl. Acad. Sci. URSS*, 30, 301.
59. Klainerman S., Majda A., 1981, *Commun. Pure Appl. Math.*, 34, 481.
60. Klainerman S., Majda A., 1982, *Commun. Pure Appl. Math.*, 35, 629.
61. Kraichnan R. H., 1965, *Phys. Fluids*, 8, 1385.
62. Kingsep, A. S., Chukbar, K. V., and Yankov, V. V. 1990, in *Reviews of Plasma Physics* (Consultant Bureau, New York) vol 16.
63. Krishan, V and Mahajan, S. M., 2004, *J. Geophys. Res.* 109, A11105.
64. Kreiss, H.-O., 1982, *Commun. Pure Appl. Math*, 33, 399439.
65. Kóta J. (2009), Paper 402-TUE-01345-0626 presented at the IAGA 11th Scientific Assembly, August 23-30, 2009, Sopron, Hungary, Programme, p.47.
66. Kowal, G., Lazarian, A., & Beresnyak, A. 2007, *ApJ*, 658, 423.
67. Krimigis S.M., D.G. Mitchell, E.C. Roelof & P.C. Brandt (2009), Presentation at "Voyagers in the Heliosheath Observations, models, and plasmas physics", January 914, Kauai, Hawaii, USA.
68. Kritsuk, A. G., Ustyugov, S. D., Norman, M. L., & Padoan, P. 2009, *Journal of Physics Conference Series*, 180, 012020.
69. Lallement R., J.L. Bertaux & F. Dalaudier. 1985, *Astron. Astrophys.*, Vol. 150, 21-32.
70. Lallement, R., et al. 2005, *Science*, 307, 1447.
71. Leamon, R.J.; Ness, N.F.; Smith, C.W.; Wong, H.K., 1999, *AIPC*, 471, 469.
72. Lee M. A. 1983, *J. Geophys. Res.*, Vol. 88, 6109.
73. Livadiotis, G., and D. J. McComas, 2009, *J. Geophys. Res.*, in press.
74. Lithwick, Y. and Goldreich, P., 2001, *Astrophys. J.*, 562, 279296.
75. Lighthill, M. J., *Proc. R. Soc. 1952, London Ser. A*, 211, 564587.
76. Lu Q. M., Q. Hu, & G. Zank (2009), *Astrophys. J.*, Vol. 706, Issue 1, pp. 687-692.
77. Majda, A.: *Compressible Fluid Flow and Systems of Conservation Laws in Several Space Variables* (Springer, New York), 1984.
78. Maron, J., & Goldreich, P. 2001, *ApJ*, 554, 1175.
79. Matthaeus, W. H., and M. Brown, 1988, *Phys Fluids*, 31, 3634.
80. Matthaeus, W. H., et al., *Phys. Rev. Lett.* 2005, 95, 231101.
81. Malama Y.G., V.V. Izmodenov & S.V. Chalov, 2006, *Astron. Astrophys.*, Vol. 445, no2, 693701.
82. Marsch E. & C.-Y. Tu (1995), *MHD structures, waves and turbulence in the solar wind: observations and theories*. Kluwer, Netherlands.
83. McKenzie J. F., & K. O. Westphal, 1969, *Planet. Space Sci.*, Vol. 17, 1029-1037.
84. McComas, D.B. Reisenfeld, N.A. Schwadron, 2010, *Astrophys. J.*, 708, 2, L126-L130.

85. McComas, D.J., F. Allegrini, P. Bochsler, M. Bzowski, M. Collier, H. Fahr, H. Fichtner, P. Frisch, H. Funsten, S. Fuselier, G. Gloeckler, M. Gruntman, V. Izmodenov, P. Knappenberger, M. Lee, S. Livi, D. Mitchell, E. Mbius, T. Moore, D. Reisenfeld, E. Roelof, N. Schwadron, M. Wieser, M. Witte, P. Wurzel, and G. Zank, 2004, The Interstellar Boundary Explorer (IBEX), Physics of the Outer Heliosphere, Third Annual IGPP Conference, AIP CP719, eds. V. Florinski, N.V. Pogorelov, G.P. Zank, 162-181.
86. McComas, D. et al., 2006, in The Physics of the Inner Heliosheath, ed.'s J. Heerikhuisen, V. Florinski, and G.P. Zank, in American Institute of Physics Conference Proceedings, AIP Conference Proceedings, Volume 858, pp. 241.
87. McComas, D. et al., 2009, Space Sci. Rev., doi:10.1007/s11214-009-9499-4.
88. McComas, D. et al., 2009, Science, 2, 10, 1126.
89. Montgomery, D. C., Brown, M. R., and Matthaeus, W. H., 1987, J. Geophys. Res., 92, 282284.
90. Mutel, R.L.; Molnar, L.A.; Spangler, S.R., 1998, American Astronomical Society, 192nd AAS Meeting, #46.13; Bulletin of the American Astronomical Society, Vol. 30, p.879.
91. Ng, C. S., Bhattacharjee, A., Germaschewski, K., & Galtier, S. 2003, Physics of Plasmas, 10, 1954.
92. Parnell C. et al. (2009), Astrophys. J., 698, 1, 75-82.
93. Pauls, H.L., G.P. Zank, L.L. Williams, 1995, J. Geophys. Res., 100, 21, 595.
94. Pauls, H.L. and G.P. Zank, 1997 J. Geophys. Res., 102, 19, 779.
95. Pogorelov, N.V., G.P. Zank, T. Ogino, 2006, Astrophys. J., 644, 1299.
96. Pogorelov, N.V., E.C. Stone, V. Florinski, G.P. Zank, 2007, Astrophys. J., 668, 611.
97. Pogorelov, N.V., J. Heerikhuisen, G.P. Zank, 2008, Astrophys. J., 675, L41.
98. N.V. Pogorelov, J. Heerikhuisen, G.P. Zank, S.N. Borovikov, 2008b, Space Sci. Rev., doi:10.1007/s11214-008-9429-x.
99. Pogorelov, N.V., Heerikhuisen, J., Zank, G.P., Borovikov, S.N., 2009, Space Sci. Rev., 143, 31
100. Pogorelov, N.V., Borovikov, S. N., Zank, G. P., & Ogino, T., 2009, Astrophys. J., 696, 1478.
101. Pogorelov, N.V., Heerikhuisen, J., Mitchel, J., Cairns, I.H., & Zank, G.P., 2009, Astrophys. J., 695, L31.
102. Prested, C.; Schwadron, N.; Passuite, J.; Randol, B.; Stuart, B.; Crew, G.; Heerikhuisen, J.; Pogorelov, N.; Zank, G.; Opher, M.; Allegrini, F.; McComas, D. J.; Reno, M.; Roelof, E.; Fuselier, S.; Funsten, H. 2008, J. Geophys. Res., 113, A6, CiteID A06102.
103. Podesta, J. J., B. D. G. Chandran, A. Bhattacharjee, D. A. Roberts, and M. L. Goldstein, 2009, J. Geophys. Res., 114, A01107, doi:10.1029/2008JA013504.
104. Pulkkinen A., Rastttter L., Kuznetsova M., Hesse M., Ridley A., Raeder J., Singer H.J. & Chulaki A. 2010, J. Geophys. Res., Vol. 115, Issue A3, CiteID A03206.
105. Richardson, J.D., et al., 2008, Nature, 454, 63.
106. Richardson, J.D., 2009, Geophys. Res. Lett., 35, CiteID L23104.
107. Saito, S., Gary, S. P., Li, H., and Narita, Y. 2008, Phys. Plasmas 15, 102305.
108. Sahraoui, F. et al. 2007, J. Plasma Physics, Vol. 73, 723.
109. Sahraoui, F. et al. 2009, Phys. Rev. Lett., Vol. 102, 231102.
110. Schwadron, N., et al., Science, 2 10.1126/science.1180986.
111. Smith, C. W., P. A. Isenberg, W. H. Matthaeus, and J. D. Richardson, 2006, Astrophys. J., 638, 508-517.
112. Shaikh, D., & Zank, G. P. 2003, Astrophys. J., 599, 715.
113. Shaikh, D., & Zank, G. P., 2005, Phys. Plasmas, 12, 122310.
114. Shaikh, D., & Zank, G. P., 2006, Astrophys. J., 640, 195.
115. Shaikh, D., & Zank, G. P., 2007, Astrophys. J., 656, 17.
116. Shaikh, D., & Shukla, P. K., 2009, Phys. Rev. Lett., 102, 045004.
117. Shaikh, D., & Shukla, P. K. 2008, FRONTIERS IN MODERN PLASMA PHYSICS: 2008 ICTP International Workshop on the Frontiers of Modern Plasma Physics. AIP Conference Proceedings, Volume 1061, pp. 66-75.
118. Shaikh, D., 2009, J. Plasma Phys., 75, 117.
119. Shaikh, D., 2009, MNRAS, 395, 2292.
120. Shaikh, D., 2010, MNRAS, 10.1111/j.1365-2966.2010.16625.x

121. Shaikh, D., 2010, Phys. Lett. A., 374, 25, 2551-2554.
122. Shaikh, D., & Zank, G. P., 2010, AIPC, 1216, 180.
123. Shaikh, D., & Zank, G. P., 2010, AIPC, 1216, 168.
124. Shaikh D, Das, A., Kaw, P., and Diamond, P. H. 2000a, Phys. Plasmas, 7 571
125. Shaikh D., Das, A., and Kaw, P. 2000b, Phys. Plasmas, 7 1366 5.
126. Schwartz S.J. et al. (2009), Experimental Astronomy, Vol. 23, Issue 3, pp.1001-1015.
127. Shinohara I. & M. Fujimoto (2009), Paper 402-TUE-01415-1055 presented at the IAGA 11th Scientific Assembly, August 23-30, 2009, Sopron, Hungary, Programme, p.54.
128. Spangler, S., Phys. Fluids, 1987, 30, 11041109.
129. Spangler, S., 1999, Astrophys. J., 522, 879896.
130. Spangler, S. R., 2001, Space Science Rev., 99, 261270.
131. Stawicki, Olaf; Gary, S. Peter; Li, Hui; 2001, JGR, 106, A5, 8273.
132. Stone, E.C., et al., 2008, Nature, 454, 71.
133. UmedaT., M. Yamao & R. Yamazaki. 2009, Astrophys. J., Vol. 695, Issue 1, pp. 574-579.
134. Veselovsky I.S. 2007, Adv. Space Res., Vol. 40, Issue 7, pp. 1087-1092.
135. Veselovsky I.S. & A.V. Prokhorov, 2008, Vol. 42, Issue 2, pp.177-182.
136. YakovchoukO.S., I.S. Veselovsky & K. Mursula. 2009, Adv. Space Res., 43, 4, 634-640.
137. Washimi, H., G.P. Zank, Q. Hu, T. Tanaka, and K. Munakata, 2007, Astrophys. J. Lett., 670, L139.
138. Williams, L.L. & G.P. Zank, 1994, J. Geophys. Res., 99, 19,229.
139. Zank, G. P. and Matthaeus, W. H., 1991, Phys. Fluids A, 3, 69-82.
140. Zank, G. P. and Matthaeus, W. H., 1993, Phys. Fluids, A5, 257-273.
141. Zank G. P., W. K. M. Rice, & C. C. Wu, 2000, J. Geophys. Res., Vol. 105, A11, 25079-25095.
142. Zank, G.P. J. Heerikhuisen, N.V. Pogorelov, R. Burrows, D. McComas, 2010, Astrophys. J., 708, Issue 2 1092-1106 doi: 10.1088/0004-637X/708/2/1092.
143. Zank, G.P., H.L. Pauls, L.L. Williams, D.T. Hall, 1996, J. Geophys. Res., 101, 21, 639.
144. Zank, G.P., H.L. Pauls, I.H. Cairns, and G.M. Webb, 1996, J. Geophys. Res., 101, 457.
145. Zank, G.P., 1999, Space Sci. Rev., 89, 413.
146. Zank, G.P., H.-R. Muller, 2003, JGR, 108, A6, 1240, doi:10.1029/2002JA009689.
147. Zank, G.P., et al., 2009, Space Sci. Rev., 146, Issue 1, 295.